Noname manuscript No.
(will be inserted by the editor)

Bearing-only Cooperative Localization

Simulation and Experimental Results

Rajnikant Sharma · Stephen Quebe · Randy Beard · Clark Taylor

Received: date / Accepted: date

Abstract In cooperative localization a group of robots exchange relative position measurements from their exteroceptive sensors and their motion information from interoceptive sensors to collectively estimate their position and heading. For the localization errors to be bounded, it is required that the system be observable, independent of the estimation technique being used. In this paper, we develop a test-bed of three ground robots, which are equipped with wheel encoders and omnidirectional cameras, to implement the bearing-only cooperative localization. The simulation and experimental results validate the observability conditions, derived in [1], for the complete observability of the bearing-only cooperative localization problem.

Keywords Cooperative Localization · Estimation Theory · Relative Position Measurement Graph · Nonlinear Observability

R. Sharma
Postdoctoral Fellow, Department of Electrical and Computer Engineering, US Air Force Academy, CO, U.S.A
E-mail: rajnikant.sharma.ctr.in@usafa.edu

S. Quebe
Graduate Research Assistant, Department of Electrical and Computer Engineering, Brigham Young University, Provo, UT, U.S.A
E-mail: squebe@gmail.com

R. Beard
Professor, Department of Electrical and Computer Engineering, Brigham Young University, Provo, UT, U.S.A
E-mail: beard@byu.edu

C. Taylor
Senior Electronics Engineer, AFRL, U.S.A
E-mail: clark.taylor@wpafb.af.mil

1 Introduction

In cooperative localization a group of robots exchange relative position measurements from their exteroceptive sensors (e.g., camera, laser, etc.) and their motion information (velocity and turn rate) from interoceptive sensors (e.g., IMU, encoders, etc.) to collectively estimate their states. Cooperative localization has been an active area of research (e.g., [2–9]) because it provides several potential advantages, including increased localization accuracy, sensor coverage, robustness, efficiency, and flexibility.

Recently, estimation algorithms such as the Extended Kalman Filter (EKF) [10], Minimum Mean Square Estimator (MMSE) [3], Maximum Likelihood Estimation (MLE) [11], Particle Filter [12], and Maximum A Posteriori (MAP) [13], have been used to solve the cooperative localization problem. These algorithms can be used either in centralized [6] or decentralized manner [3,10,13]. For the localization errors to be bounded, it is required that the system be observable, independent of the estimation technique being used.

Several authors have carried out observability analysis of the cooperative localization problem. Initial results regarding the observability of cooperative localization were reported by Roumeliotis and Bekey [10]. They used linear observability analysis to show that the states of the robots performing cooperative localization are unobservable, but can be made observable by providing global positioning information to one of the robots. In [10] it was assumed that the absolute vehicle heading is measured directly and does not need to be estimated. Furthermore, linear approximation of a nonlinear system can provide different structural properties regarding the observability [14,15]. Martinelli *et al.* [16] investigates the nonlinear observability of cooperative

localization for two robots without heading measurements. They compared the observability properties of range and bearing measurements and showed that with either type of measurement, the maximum rank of the observability matrix is three, i.e., not fully observable. The analysis in [16] shows that relative bearing is the best observation between the robots. The part of the system which is observable is in general larger than for the other relative observations (relative distance and relative orientation). Accordingly, [16] uses polar coordinates for the observability analysis.

In our previous work [1], we have extended the observability analysis presented in [16] from 2 to n robots, with bearing-only measurements. The extension for $n > 2$ is not obvious because of the dynamically changing set of $n(n-1)/2$ different relative bearing measurements leading to $2^{n(n-1)/2}$ possible configurations. Furthermore, since the robot states in [16] are not observable with respect to a global reference frame, and since it has been shown that two landmarks are needed for the observability of a single vehicle [17–19], in [1] we have derived the number of landmarks needed for full observability of a group of n robots performing cooperative localization. In contrast to [10], we have assumed that the heading of each robot is not directly measured but must be estimated.

In [1], we have used the Relative Position Measurement Graph (RPMG) to represent a group of robots. The nodes of an RPMG represent vehicle states and the edges represent bearing measurements between nodes. We have established a relationship between the graph properties of the RPMG and the rank of the system observability matrix. We have proved that for a connected RPMG, the observability matrix for a team of n robots, which has size $3n \times 3n$ will have rank $3(n-1)$. We also derive conditions under which landmarks observed by a subset of robots enable the system to become fully observable.

In this paper, we develop a test-bed of three ground robots, which are equipped with wheel encoders and omnidirectional cameras, to implement the bearing-only localization. We present simulation and experimental results to validate the observability conditions [1] for the complete observability of the bearing-only cooperative localization problem.

The paper is organized as follows. In Section 2 we describe bearing-only cooperative localization and formulate the problem. In Section 3 we summarize the observability analysis results obtained in [1]. The simulation and experimental results are presented in Section 4. In Section 5 we give our conclusions.

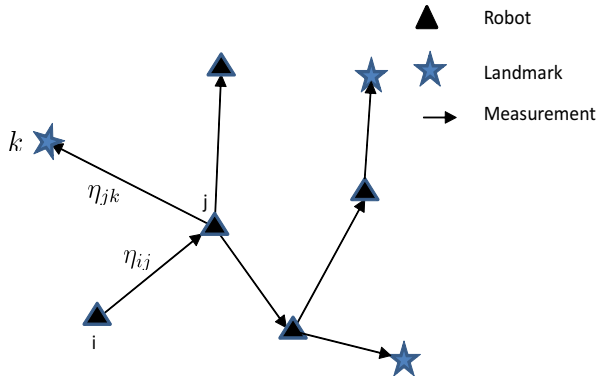

Fig. 1 Relative position measurement graph (RPMG). The nodes of an RPMG represent vehicle states and the edges represent bearing measurements between nodes.

2 Bearing-only Cooperative Localization

Consider n robots moving in a horizontal plane performing cooperative localization. We can write the equations of motion for the i^{th} robot as

$$\dot{X}_i = f_i(X_i, u_i) \triangleq \begin{pmatrix} V_i \cos\psi_i \\ V_i \sin\psi_i \\ \omega_i \end{pmatrix}, \tag{1}$$

where $X_i = [x_i \ y_i \ \psi_i]^\top \in \mathbb{R}^3$ is the robot state, including robot location $(x_i, \ y_i)$ and robot heading ψ_i, and $u_i = [V_i, w_i]^\top$ is the control input vector. We assume that onboard introspective sensors (e.g., encoders) measure the linear speed V_i and angular speed ω_i of the robot. Without loss of generality, we assume that robots cannot move backward ($V_i \geq 0, \ i = 1 \cdots n$). Each vehicle has an exteroceptive sensor to measure relative bearing to other vehicles and known landmarks that are in the field-of-view of the sensor. Relative bearing from the i^{th} robot to the j^{th} robot or landmark can be written as

$$\eta_{ij} = \tan^{-1}\left(\frac{y_j - y_i}{x_j - x_i}\right) - \psi_i. \tag{2}$$

For cooperative localization, each robot exchanges its local sensor measurements (velocity, turn rate, and bearing to landmarks and other robots) with their neighbors. Let N_i^M be the set of neighbors for which robot i can obtain bearing measurements, and let N_i^C be the set of neighbors with which robots i can communicate. In this paper, we assume that $N_i^M = N_i^C$ and we will therefore denote the set of neighbors as N_i. To represent the connection topology of the robots we use a relative position measurement graph (RPMG) [20] which is defined as follows.

Definition 1 An RPMG for n robots performing cooperative localization with l different known landmarks

is a directed graph $G_n^l \triangleq \{\mathcal{V}_{n,l}, \mathcal{E}_{n,l}\}$, where $\mathcal{V}_{n,l} = \{1, \cdots, n, n+1, \cdots, n+l\}$ is the node set consisting of n robot nodes and l landmark nodes and $\mathcal{E}_{n,l}(t) \subset \{\mathcal{V}_{n,0} \times \mathcal{V}_{n,l}\} = \{\eta_{ij}\}$, $i \in \{1, \cdots, n\}$, $j \in \{1, \cdots, n, n+1, \cdots, n+l\}$ is the edge set representing the availability of a relative bearing measurement. We use m to denote the number of edges in the RPMG. An example RPMG (G_5^3 with $m = 7$) is shown in Fig. 1.

Additionally, without loss of generality we assume that robots maintain a safe distance from each other and from landmarks, i.e., $R_{ij} > 0$, $\forall i, j = 1, \cdots n$ and landmarks $R_{ik} > 0$, $\forall i = 1, \cdots n$; $k = 1, \cdots, l$.

2.1 Cooperative Localization implementation

The objective of the cooperative localization is to estimate the combined state $\hat{X}(k) = [\hat{X}_1(k), \cdots, \hat{X}_n(k)]^\top$. We use an extended information filter(EIF) to implement the bearing-only cooperative localization. In the information filter instead of state $\hat{X}$ and covariance $P(k)$ the information vector $\hat{y}(k)$ and information matrix $Y(k)$ is updated. The information matrix and information vector can be computed as

$$Y(k) = P(k)^{-1} \tag{3}$$

$$\hat{y}(k) = Y(k)\hat{X}(k) \tag{4}$$

Similar to an extended kalman filter (EKF) the EIF has two steps. The first is the prediction step, which is given below.

$$Y(k+1|k) = (F(k)Y(k|k)^{-1}F(k)^\top + B(k)Q(k)B(k)^\top)^{-1} \tag{5}$$

$$\hat{y}(k+1|k) = Y(k+1|k)\hat{X}(k+1|k) \tag{6}$$

$$\hat{X}(k+1|k) = X(k|k) + T_s f(\hat{X}(k|k), u(k)) \tag{7}$$

where $F_k = \begin{pmatrix} F_1 & 0 & \cdots & 0 \\ 0 & F_2 & \cdots & 0 \\ \vdots & \cdots & \ddots & 0 \\ 0 & 0 & \cdots & F_n \end{pmatrix}$, $B(k) = \begin{pmatrix} B_1 \\ \vdots \\ B_n \end{pmatrix}$, and $Q(k) = \begin{pmatrix} Q_i(k) & 0 & 0 \\ 0 & \ddots & 0 \\ 0 & 0 & Q_n(k) \end{pmatrix}$ is covariance of noise in the control input. The matrix F_i and B_i are the system jacobian with respect to state X_i and control u_i, which are given below

$$F_i = I_3 + T_s \frac{\partial f_i}{\partial X_i}|_{X_i = X_i(k)} = \begin{bmatrix} 1 & 0 & -V_i T_s \sin\psi(k) \\ 0 & 1 & V_i T_s \cos\psi(k) \\ 0 & 0 & 1 \end{bmatrix}, \tag{8}$$

$$B_i = T_s \frac{\partial f_i}{\partial u_i}|_{u_i = u_i(k)} \begin{bmatrix} T_s\cos\psi_k & 0 \\ T_s \sin\psi_k & 0 \\ 0 & T_s \end{bmatrix}, \tag{9}$$

and $Q_i(k) = \begin{pmatrix} \sigma_{v_i}^2 & 0 \\ 0 & \sigma_{\omega_i}^2 \end{pmatrix}$, where σ_{v_i} and σ_{ω_i} are the standard deviation in velocity input and turn rate input respectively.

The measurement update step is given as

$$Y(k+1|k+1) = Y(k+1|k) + \sum H_{ij}(k)^\top \sigma_{\eta_{ij}}^{-2} H_{ij}(k)$$

$$\hat{y}(k+1|k+1) = \hat{y}(k+1|k) \cdots + \sum H_{ij}(k)^\top R_{ij}^{-1}(\mu_{ij} + H_{ij}\hat{X}(k+1|k))$$

The scalar μ_{ij} represents the innovation

$$\mu_{ij} = \eta_{ij} - h_{ij}(x(k+1|k)) \tag{10}$$

and $\sigma_{\eta_{ij}}$ is standard deviation of the noise in the bearing measurement. The row vector H_{ij} is the measurement jacobian

$$H_{ij}(k) = \frac{\partial h_{ij}}{\partial X}|_{X = X(k)}. \tag{11}$$

The EIF is dual of the EKF and the EKF is a quasi-local asymptotic observer for nonlinear systems and its convergence and boundedness are achieved when the system is fully observable [21].

2.2 Lie Derivatives and Nonlinear Observability

To determine the observability of the entire system represented by the RPMG we use the nonlinear observability rank criteria developed by Hermann and Krener [22] which is summarized in the next paragraph.

Consider a system model with the following form

$$\Sigma : \begin{matrix} \dot{X} = f(X, u) = [f_1^\top(X_1, u_1), \cdots, f_n^\top(X_n, u_n)]^\top \\ y = h(X, Z) = [h_1^\top(X, Z) \cdots h_m^\top(X, Z)]^\top \end{matrix} \tag{12}$$

where $X = [X_1^\top X_2^\top \cdots X_n^\top]^\top \in \mathbb{R}^{3n}$ is the state of the system, $Z = [Z_1^\top Z_2^\top \cdots Z_l^\top]^\top \in \mathbb{R}^{2l}$ is the position vector of all landmarks, $Z_i = [x_i\ y_i]^\top$ is the position vector of i^{th} landmark, $h_i : \mathbb{R}^{3n} \times \mathbb{R}^{2l} \mapsto \mathbb{R}$ is the measurement model of the i^{th} sensor, $u \in \Lambda \subseteq \mathbb{R}^{2n}$ is the control input vector, and $g : \mathbb{R}^{3n} \times \Lambda \mapsto \mathbb{R}^{3n}$. We consider the

special case where the process function g can be separated into a summation of independent functions, each one excited by a different component of the control input vector, i.e.,

$$\dot{X} = f(X,u) = f_{v_1}V_1 + f_{\omega_1}\omega_1 + \cdots + f_{v_n}V_n + f_{\omega_n}\omega_n \tag{13}$$

The zeroth-order Lie derivative of any (scalar) function is the function itself, i.e., $L^0 h_k(X,Z) = h_k(X,Z)$. The first-order Lie derivative of function $h_k(X,Z)$ with respect to f_{v_i} is defined as

$$L^1_{f_{v_i}} h = \nabla L^0 h \cdot f_{v_i} \tag{14}$$

∇ represents the gradient operator, and $\cdot$ denotes the vector inner product. Considering that $L^1_{f_{v_i}} h_k(X,Z)$ is a scalar function itself, the second-order Lie derivative of $h_k(X,Z)$ with respect to f_{v_i} is

$$L^2_{f_{v_i} f_{v_i}} h = \nabla L^1_{f_{v_i}} h \cdot f_{v_i}. \tag{15}$$

Higher order Lie derivatives are computed similarly. Additionally, it is possible to define mixed Lie derivatives, i.e., with respect to different functions of the process model. For example, the second-order Lie derivative of h_k with respect to f_{v_j}, given its first derivative with respect to f_{v_i}, is

$$L^2_{f_{v_i} f_{v_j}} h = \nabla L^1_{f_{v_i}} h \cdot f_{v_j}. \tag{16}$$

Based on the preceding expressions for the Lie derivatives the observability matrix is defined as the matrix with rows

$$\mathcal{O} = \left\{ \nabla L^p_{f_{v_i},\cdots,f_{v_j},f_{\omega_i},\cdots,f_{\omega_j}} h_k(X,Z) \right\} \tag{17}$$

where $i,j = 1,\cdots,n; k = 1,\cdots,m; p \in \mathbb{N}$. The important role of this matrix in the observability analysis of a nonlinear system is demonstrated by Theorem 1.

Theorem 1 *A system is locally weakly observable if its observability matrix whose rows are given in* (17) *has full rank, e.g., in our case rank*$(\mathcal{O}) = 3n$.

Additionally, we assume that the robot sensors have limited sensor range ρ_{sensor} and limited field of view. Therefore, agents can only measure the bearing of those robots and landmarks that are located within the footprint of the sensor. Therefore, the graph G^l_n will likely have a time varying topology.

3 Graph-based Observability Analysis

In this section, we summarize the conditions for the observability of the graph G^l_n derived in [1]. In a graph G^l_n there are two types of edges: an edge between two robots, and an edge between a robot and a landmark. The linearly independent rows of the observability submatrix of an edge serve as building block for the observability conditions for the graph G^l_n.

The observability matrix of an edge between two robots can be written using gradients of Lie derivatives (detailed derivation is given in [1]) up to second-order as

$$\mathcal{O}_{ij} = \begin{bmatrix} -\Delta y_{ij} & \Delta x_{ij} & -R^2_{ij} & \Delta y_{ij} & -\Delta x_{ij} & 0 \\ s\psi_i & -c\psi_i & J^+_i & -s\psi_i & c\psi_i & 0 \\ -s\psi_j & c\psi_j & 0 & s\psi_j & -c\psi_j & -J^+_j \\ -2\Delta x_{ij} & -2\Delta y_{ij} & 0 & 2\Delta x_{ij} & 2\Delta y_{ij} & 0 \\ 0 & 0 & -J_\psi & 0 & 0 & J_\psi \\ c\psi_i & s\psi_i & J^-_i & -c\psi_i & -s\psi_i & 0 \\ -c\psi_j & -s\psi_j & 0 & c\psi_j & s\psi_j & -J^-_j \end{bmatrix}. \tag{18}$$

The next lemma provides conditions for the maximum rank of the observability matrix of an edge between two robots.

Lemma 1 ([1]) *The rank of* $\mathcal{O}_{ij}$ *given by* (18) *(edge between two robots) is three if*

1. $V_i > 0$,
2. $V_j > 0$,
3. *the* i^{th} *robot, which is measuring the bearing, does not move along the line joining the two robots,*
4. *the* j^{th} *robot does not move perpendicular to the line joining the two robots.*

Similarly, the observability matrix corresponding to an edge between a robot and a landmark, using the gradients of Lie derivatives up to second order, as

$$\mathcal{O}_{ik} = \begin{bmatrix} -\Delta y_{ik} & \Delta x_{ik} & -R^2_{ik} \\ s\psi_i & -c\psi_i & J^+ \\ -2\Delta x_{ik} & -2\Delta y_{ik} & 0 \\ c\psi_i & s\psi_i & J^- \end{bmatrix} \tag{19}$$

where $J^+ = \Delta x_{ik} c\psi_i + \Delta y_{ik} s\psi_i$ and $J^- = \Delta y_{ik} c\psi_i - \Delta x_{ik} s\psi_i$.

Lemma 2 ([1]) *The rank* O_{ik} *given by* (19) *(edge between a robot and a landmark) is two if*

1. $V_i > 0$,
2. *the robot does not move along the line joining the robot and the landmark.*

Next, we define a proper RPMG.

Definition 2 An RPMG G_n^l (Definition 1) is called a proper RPMG if all the edges between robot nodes satisfy the conditions of Lemma 1 and all the edges between robots and landmarks satisfy Lemma 2.

Next, theorem, which is proved in [1], summarize the observability conditions for a proper RPMG G_n^0 without any landmarks.

Theorem 2 ([1]) *If the graph G_n^0 is a proper connected RPMG then the rank of the associated observability matrix is $3(n-1)$.*

It should noted that the maximum rank of the observability matrix of RPMG G_n^0 without any landmarks is less then $3n$, therefore, the system in not completely observable. Next theorem provides the conditions for the complete observability of the system in the presence of known landmarks.

Theorem 3 ([1]) *Given a proper RPMG G_n^l, if for each robot there exists a path to at least two landmarks and the robot and two landmarks are not on the same line (i.e., $\eta_{i1} \neq \eta_{i2}, \forall\ i = 1, \cdots, n$) then the system is completely observable, i.e., the rank of the observability matrix is $3n$.*

An alternative method for obtaining complete observability without landmarks is derived in the nest theorem.

Theorem 4 *Given a RPMG G_n^0, if it is proper, connected, and one of the robot has its position and heading measurement from GPS then the system is completely observable, i.e., the rank of the observability matrix is $3n$.*

Proof If RPMG G_n^0 is proper and connected then from Theorem 2 there are $3(n-1)$ linearly independent rows in the observability matrix and if one of the robot measures its position and heading directly from a GPS receiver then three linearly independent rows, which are linearly independent to the existing $3(n-1)$ rows, are added. Therefore, the rank of the observability matrix becomes $3n$ and system becomes completely observable.

4 Results

In this section, we present simulation and hardware results to validate the observability conditions discussed in the previous section.

4.1 Simulation Results

The simulation environment consists of five homogenous ground robots and two landmarks. Each robot is equipped with an encoder, which provides the robot's linear and rotation velocities, and a omini-directional camera, which measure bearing from other robots and landmarks in the sensor range R_{sensor}. We assume that the noise in encoder and camera measurement are Gaussian. Following are the different simulation parameters of a robot used in the simulation results presented in this paper.

- Sensing range of the omni-directional camera ($R_{sensor} = 120m$).
- Linear velocity of the robot ($V = 5\ m/s$).
- Sampling time period $T_s = 0.1\ s$.
- Initial pose uncertainty ($\sigma_{x0}\ \sigma_{y0}\ \sigma_{\psi_0}] = [5m\ 5m\ 0.2rad]$).
- Standard deviations of process noise in encoder $[\sigma_v\ \sigma_\omega]^T = [0.2m/s\ 0.2rad/s]^T$.
- Standard deviation of measurement noise $\sigma_{\eta_{ij}} = 0.1rad$.

To numerically prove the Theorem 3, we define a metric for the existence of a path between two nodes in the RPMG. For this, we make use of the ideas of k-connectivity [23].

The adjacency matrix of a proper RPMG can be defined as $A = [a_{ij}] \in R^{(n+l)\times(n+l)}$ where

$$a_{ij} = \begin{cases} 1\ if\ \ \sin\eta_{ij}(R_{sensor} - R_{ij}) > 0\ and\ i\ \in [1,n] \\ 0\ otherwise \end{cases} \tag{20}$$

The k-connectivity matrix is defined as

$$C_k \triangleq I_{n+l} + A + A^2 + \cdots + A^k \tag{21}$$

and the entry $C_k(i,j)$ can be interpreted as the number of paths of k-hops or less that connect node i to node j. Next we define a metric $\beta(G_n^2)$ for RPMG with two landmarks which summarizes all of the conditions in Theorem 3.

$$\beta(G_n^2) = \begin{cases} 1\ if\ \ \prod_{1=1,n} C_n(i,n+1)C_n(i,n+2) > 0 \\ 0\ otherwise \end{cases} \tag{22}$$

From Theorem 3 we can say that if $\beta(G_n^2) = 1$ then the system is completely observable. In Fig. 2, we plot the smallest singular value of the actual nonlinear observability matrix and $\beta(G_5^2)$. It can be seen that when $\beta(G_5^2) = 1$ then each robot node in RPMG has path to two landmarks and the system is completely observable. On the other hand, when $\beta(G_5^2) = 0$ then all of the robots in the do not have path to two landmarks

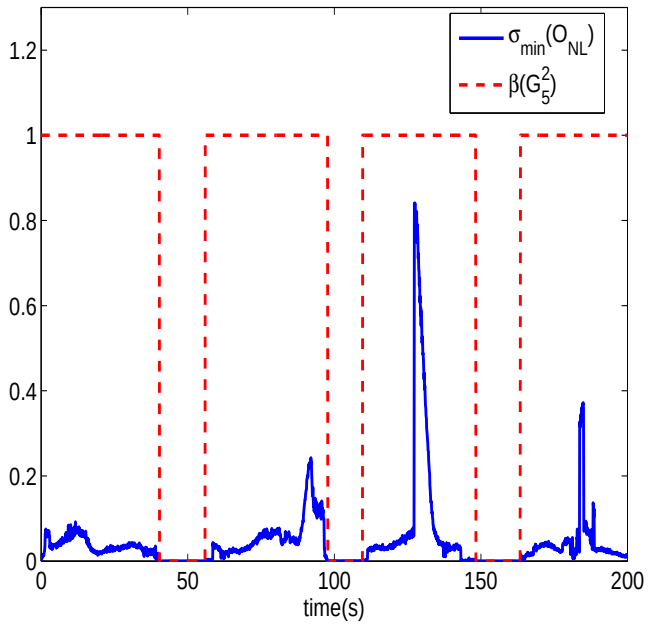

Fig. 2 Connectivity vs Observability: The dashed red curve represents the connectivity, of a RPMG with five robots and two landmarks, as defined in (22). The solid blue curve represents the smallest singular value of the nonlinear observability matrix as defined in (17). When $\beta(G_5^2) = 1$ then each robot node in RPMG has path to two landmarks and the system is completely observable. On the other hand, when $\beta(G_5^2) = 0$ then all of the robots in the do not have path to two landmarks and system is unobservable.

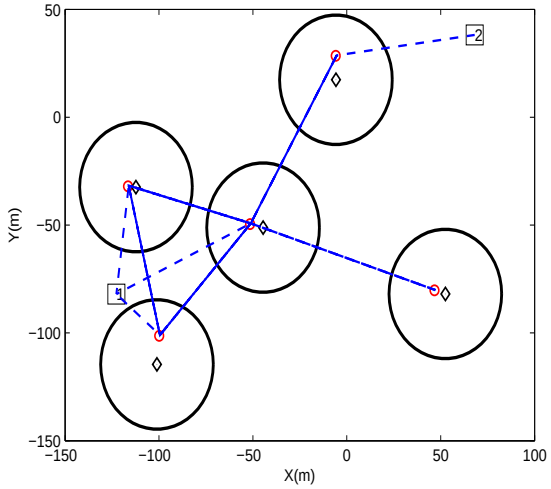

Fig. 3 Initial topology for bearing-only cooperative localization. The black circles represent the initial position uncertainty (3σ). The black diamonds represent the initial position estimates of robots. The red circles are the true initial positions of the robots. The dashed blue line represents an edge (bearing measurement) between two nodes. Two numbered squares are the two known landmarks.

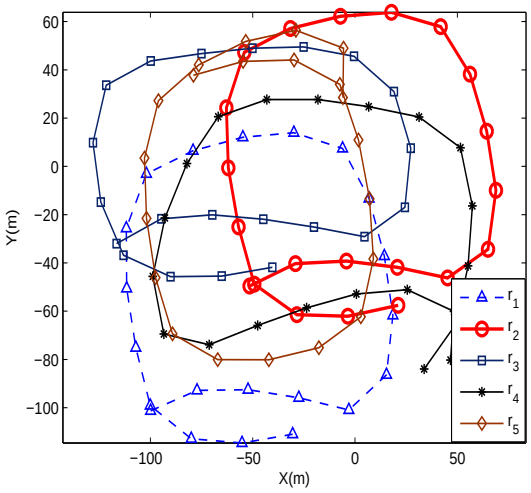

Fig. 4 True trajectories of all of the five robots. The trajectories are generated by following way-points, and the way-points are chosen such that the RPMG G_5^2 remains connected.

and system is unobservable. This numerically proves the Theorem 3.

We run the bearing-only cooperative localization algorithm for four different cases. In the first case the measurements from the landmarks are not used for estimation. In the second case bearing measurements from only one landmark are considered, and in the third case bearing measurements from two landmarks are considered. Finally, we do not consider any landmarks, however, the absolute position and heading of a robot from a GPS receiver are fused with inter robot bearing measurements to perform the cooperative localization. The Fig. 3 shows the initial topology of the RPMG with five robots and two landmarks. Initially, the RPMG is connected and the waypoints for all of the five robots are chosen such that the RPMG is remains connected. The actual trajectories of all of the five robots is shown in Fig. 4, and the Fig 5 shows the true and estimated trajectories of the second robot, for all of the four cases. It can be seen that estimated trajectories for CL with two landmarks and GPS (first robot) are closest to the true trajectory. The comparison for position error (second robot) for all the four cases is shown in Fig 6 and Fig. 7.

Fig 8, Fig. 9, and Fig. 10 show the plots for the second robot's estimated uncertainty (3σ) in X, Y, and ψ respectively for all of the four cases. It can be seen that the uncertainty for two landmarks and GPS case is lower then the uncertainty related to no landmark and one landmark. This is because with two landmarks or absolute position and heading measurement of a robot from GPS the system is observable.

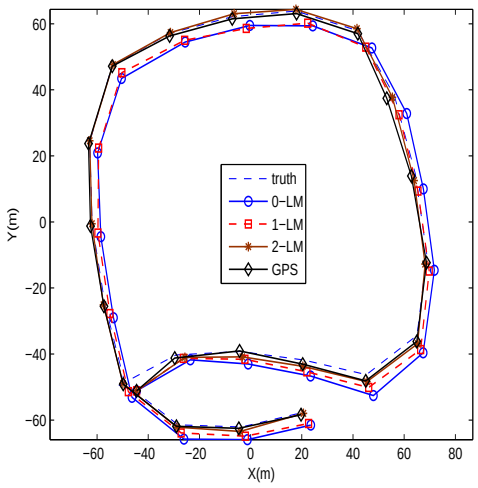

Fig. 5 The second robot trajectories:(1) The true trajectory is represented by the dashed curve. (2) The estimated trajectory using CL with no landmarks is represented by solid curve with circles.(3) The estimated trajectory using CL with only one landmarks is represented by the solid curve with squares. (4)The estimated trajectory using CL with two landmarks is represented by the solid curve with stars. (5) The estimated trajectory using CL, when Robot 1's position and attitude is measured using a GPS, is represented by the solid curve with diamonds.

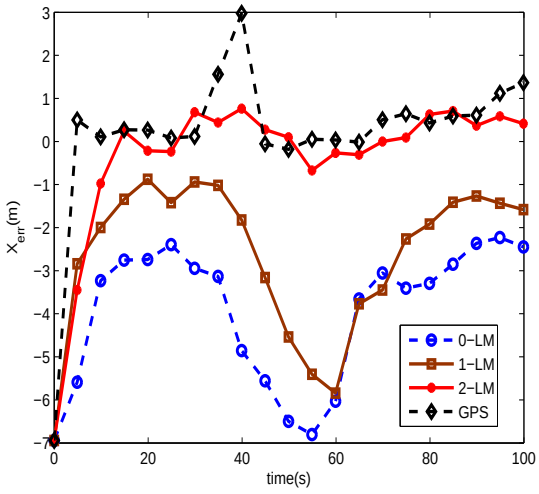

Fig. 6 The comparison of second robot's error in X direction. This figure shows the plots of error in X direction with no landmark, one landmark, two landmark, and with GPS measurements of the Robot 1. The error with no landmark and one landmark is higher than error with two landmarks and GPS because in last two case the system is observable.

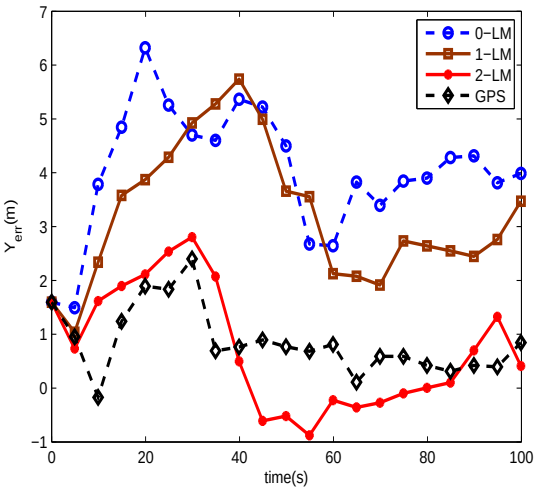

Fig. 7 The comparison of second robot's error in Y direction. This figure shows the plots of error in Y direction with no landmark, one landmark, two landmark, and with GPS measurements of the Robot 1. The error with no landmark and one landmark is higher than error with two landmarks and GPS because in last two case the system is observable.

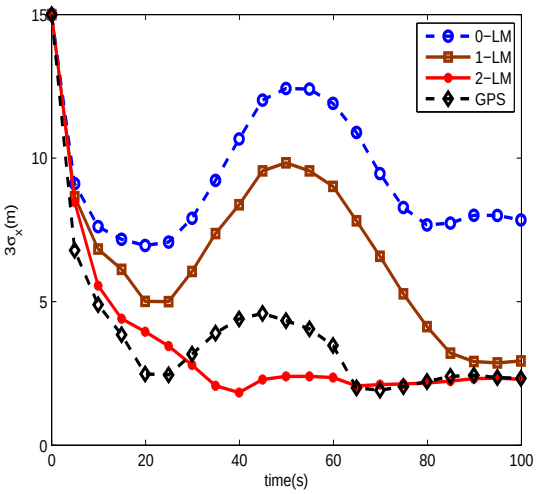

Fig. 8 The comparison of second robot's estimation uncertainty($3\sigma_x$) in X direction. This figure shows the plots of error covariance in X direction with no landmark, one landmark, two landmark, and with GPS measurements of the Robot 1. The error with no landmark and one landmark is higher than error with two landmarks and GPS because in last two case the system is observable.

4.2 Experimental Results

For experimental validation we use three stinger robots (see Fig. 11) with serializer controller. For turn rate and velocity measurement wheel encoders are used. For bearing measurement we use an omnidirectional camera and an EEE pc for onboard processing and communi-

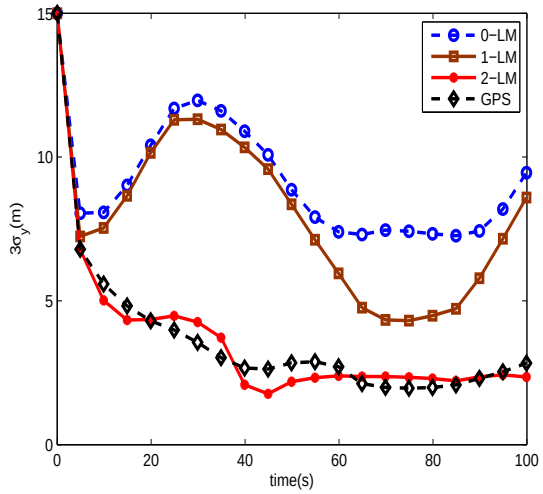

Fig. 9 The comparison of second robot's estimation uncertainty ($3\sigma_y$) in Y direction. This figure shows the plots of error covariance in Y direction with no landmark, one landmark, two landmark, and with GPS measurements of the Robot 1. The error with no landmark and one landmark is higher than error with two landmarks and GPS because in last two case the system is observable.

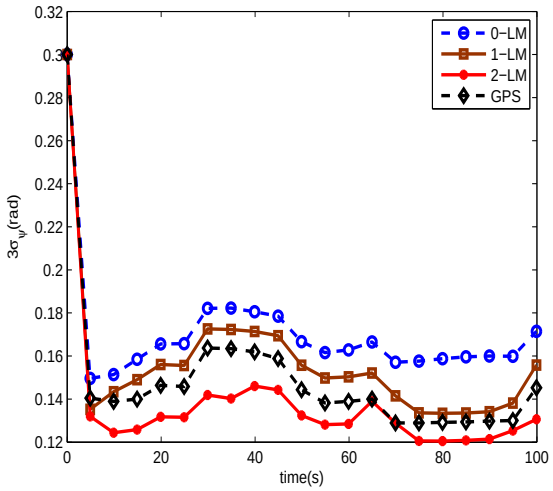

Fig. 10 The comparison of second robot's estimation uncertainty ($3\sigma_{psi}$) in heading. This figure shows the plots of error covariance in ψ direction with no landmark, one landmark, two landmark, and with GPS measurements of the Robot 1. The error with no landmark and one landmark is higher than error with two landmarks and GPS because in last two case the system is observable.

cation. The experimental setup is shown in Fig. 12. It consist of three robots with different color (green, blue, and orange) for their identification. The snapshot of the experimental area taken from the omnidirectional camera on the orange robot is shown in Fig. 13. The robots communicate with each other on a wireless network using a router. We use an overhead camera to obtain the true robot states and compare the estimated states. We use color segmentation to find the bearing of the robots and landmarks which are in the image plane of a omnidirectional camera.

To do cooperative localization, the robots needed a reliable method of exchanging information with one another. To meet this need we designed a software system that enabled multiple agents to discover and reliably communicate with one other over a small local area network. We called this system the Agent Management System. In the Agent Management System each robot was represented by a single software construct we called a Software Agent. The Software Agent was a single process, run on the robot's onboard computer that concurrently managed the robot's processing and communication. There were two core elements that enabled the Software Agents to communicate reliably. The first element was peer discovery. The second was message handling. Peer discovery enabled the Software Agents to find each other maintain an active directory of all other agents that it could communicate with. As soon as a Software Agent process started, it began listening for and periodically broadcasting a short discovery message across the local area network. When another Software Agent heard one of these messages, it sent back a reply informing the sending agent its contact information (an IP address and port number). Within a short period of time all software agents had a list of every active agent on the network. Each agent would continue pinging each other (at a less frequent interval) if the neighboring robot failed to reply to a certain number of pings, it was removed from the list of available robot's to communicate with. With a reliable list of neighboring agents to communicate with, the agents were able to start sending information back and forth between each other. Each message was serialized and sent as a single UDP packet. When received, the Software Agent would put the messages in a single message queue that could be read from and processed. We elected to use the UDP protocol because we needed small rapid measurements from each robot in order to make good cooperative estimates. Using the Agent Management System, we were able to design, test, and record our experiment for cooperative navigation and control.

Following parameters are used for the experiment

- Linear velocity of the robot ($V = 0.2\ m/s$).
- Sampling time period $T_s = 0.1\ s$.
- Standard deviations of process noise in encoder $[\sigma_v\ \sigma_\omega]^T = [0.08m/s\ 0.12rad/s]^T$.
- Standard deviation of measurement noise $\sigma_{\eta_{ij}} = 0.13rad$.

Fig. 14 shows the trajectory of all of the three robots, which are computed (1) using only encoders, (2)using

Fig. 11 The Stinger robot. This robot is equipped with a serialize controller, two wheel encoders, an omnidirectional camera, and Asus EEE computer.

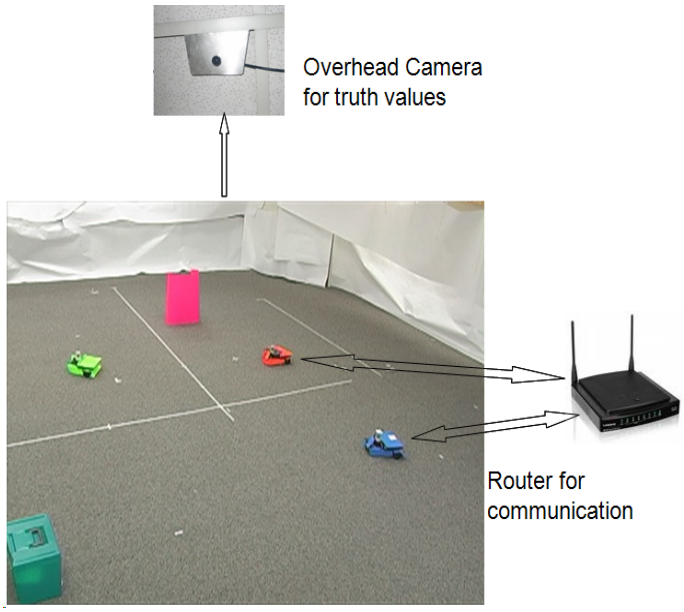

Fig. 12 Experimental setup with three ground robots (orange, light green, and blue) and two landmarks (pink and dark green boxes). The robots and the landmarks are identified from their color. The robots communicate with each using the TCP-IP protocol over a communication router. Each robot shares its bearing measurements (measured using omnidirectional camera) and linear and rotational velocities (measured by two wheel encoders) with the the other robots in the group. The truth position and heading of all of the robots computed using the overhead camera.

bearing-only cooperative localization, and (3)using the overhead camera. It can be seen that the trajectories computed using bearing only cooperative localization are closer to the trajectories computed using the overhead camera. The estimation error plots (X, Y, and ψ) of the blue robot are shown in Fig. 15, 16, and 17. It can be seen that the estimation error of all of the states using bearing-only cooperative localization with two landmarks is bounded, however, the estimation error using only encoder measurement drifts.

Additional videos of simulation and experimental results related to bearing-only cooperative localization can be found in [24].

5 Conclusion

In this paper, we develop a test-bed of three ground robots, which are equipped with wheel encoders and omnidirectional cameras, to implement the bearing-only cooperative localization. The simulation and experimental results validate the observability conditions, derived in [1], for the complete observability of the bearing-only cooperative localization problem.

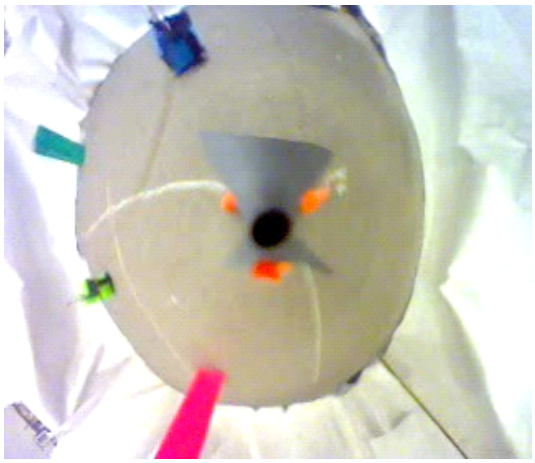

Fig. 13 This figure shows the omnidirectional camera snap shot taken from the orange robot. The snap shot shows the 360^o view of the the experimental area. It can be seen that other two robots and two landmarks are clearly visible in the image plane. The bearing from the robots and landmarks in the image plane can computed using color segmentation.

References

1. R. Sharma, R. Beard, C. N. Taylor, and S. Quebe, "Graph-based observability analysis of bearing-only cooperative localization," *IEEE Transaction On Robotics*, vol. 28, 2, 2011.
2. R. Kurazume and S. Hirose, "Study on cooperative positioning system: optimum moving strategies for CPS-III," in *Proc. IEEE International Conference on Robotics and Automation*, vol. 4, 16–20 May 1998, pp. 2896–2903.

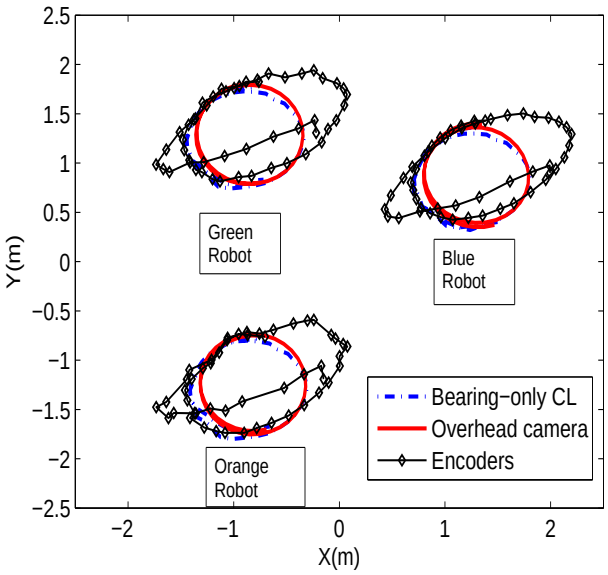

Fig. 14 Trajectories of three robots. There are three different trajectories for each robot including trajectory computed from over head camera (red solid curve), estimated trajectory using encoder measurement only (black solid curve with diamonds), and estimated trajectory using bearing-only cooperative localization (blue dotted curve).

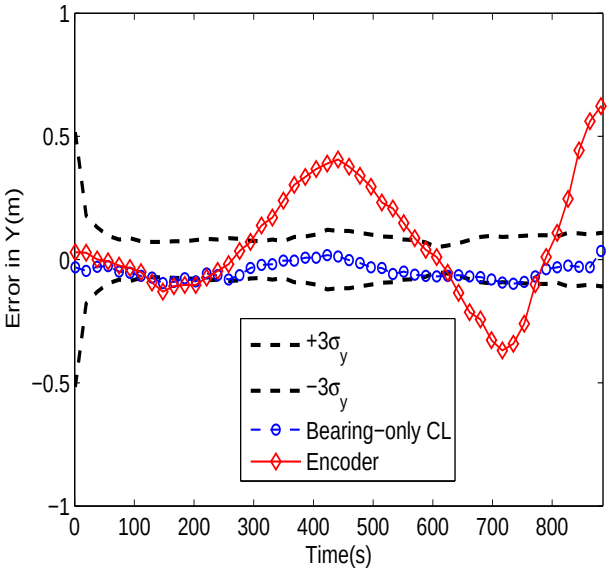

Fig. 16 Error in X direction of the blue robot:The dashed black curve represents the $\pm 3\sigma_y$ uncertainty. The estimation error in Y direction using encoder measurements is represented by the red solid curve with diamonds, and the estimation in Y direction using bearing-only measurements is represented by the blue solid curve with circles.

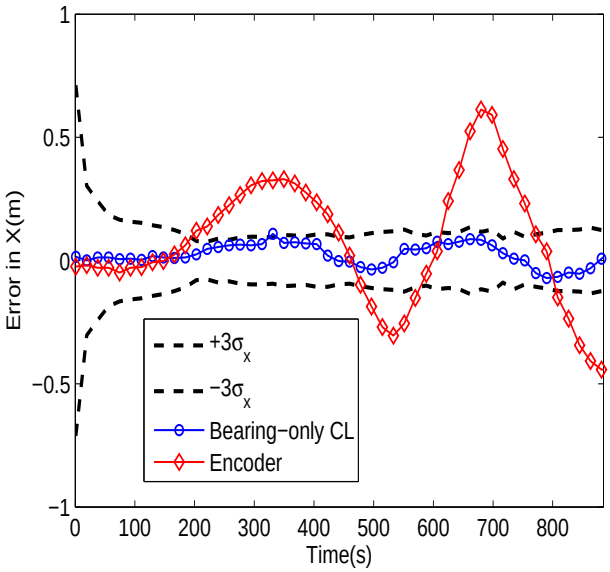

Fig. 15 Error in X direction of the blue robot:The dashed black curve represents the $\pm 3\sigma_x$ uncertainty. The estimation error in X direction using encoder measurements is represented by the red solid curve with diamonds, and the estimation in X direction using bearing-only measurements is represented by the blue solid curve with circles.

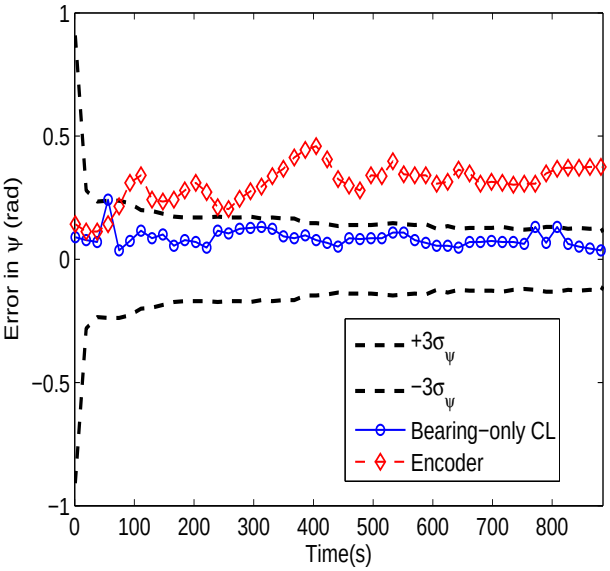

Fig. 17 Error in heading of the blue robot:The dashed black curve represents the $\pm 3\sigma_\psi$ uncertainty. The estimation error in heading using encoder measurements is represented by the red solid curve with diamonds, and the estimation error in heading using bearing-only measurements is represented by the blue solid curve with circles.

3. A. C. Sanderson, "A distributed algorithm for cooperative navigation among multiple mobile robots," *Advanced Robotics*, vol. 12, pp. 335–349, 1998.
4. S. I. Roumeliotis and G. A. Bekey, "Collective localization: a distributed kalman filter approach to localization of groups of mobile robots," in *Proc. IEEE International Conference on Robotics and Automation ICRA '00*, vol. 3, 24–28 April 2000, pp. 2958–2965.
5. J. Spletzer, A. Das, R. Fierro, C. Taylor, V. Kumar, and J. Ostrowski, "Cooperative localization and control for multi-robot manipulation," in *Proc. IEEE/RSJ International Conference on Intelligent Robots and Systems*, vol. 2, 2001, pp. 631–636 vol.2.
6. I. M. Rekleitis, G. Dudek, and E. E. Milios, "Multi-robot cooperative localization: a study of trade-offs between efficiency and accuracy," in *Proc. IEEE/RSJ International Conference on Intelligent Robots and System*, vol. 3, 30 Sept.–5 Oct. 2002, pp. 2690–2695.
7. P. Nebot, D. Gomez, and E. Cervera, "Agents for cooperative heterogeneous mobile robotics: a case study," in *Proc. IEEE International Conference on Systems, Man and Cybernetics*, vol. 1, 5–8 Oct. 2003, pp. 557–562.
8. A. Bahr, J. J. Leonard, and M. F. Fallon, "Cooperative localization for autonomous underwater vehicles," *International Journal of Robotics Research*, vol. Volume 28 , Issue 6, pp. 714–728, 2009.
9. A. Mourikis and S. Roumeliotis, "Analysis of positioning uncertainty in reconfigurable networks of heterogeneous mobile robots," in *Proc. IEEE International Conference on Robotics and Automation ICRA '04*, vol. 1, 2004, pp. 572–579 Vol.1.
10. S. I. Roumeliotis and G. A. Bekey, "Distributed multirobot localization," *IEEE Transaction for Robotics and Autonomus Systems*, vol. 18, no. 5, pp. 781–795, 2002.
11. A. Howard, M. J. Matark, and G. S. Sukhatme, "Localization for mobile robot teams using maximum likelihood estimation," in *Proc. IEEE/RSJ Int Intelligent Robots and Systems Conf*, vol. 1, 2002, pp. 434–439.
12. D. Fox, W. Burgard, H. Kruppa, and T. S, "A probabilistic approach to collaborative multi-robot localization," *Autonomous Robots*, vol. 8, pp. 325–344, 2000.
13. E. D. Nerurkar, S. I. Roumeliotis, and A. Martinelli, "Distributed maximum a posteriori estimation for multi-robot cooperative localization," in *Proc. IEEE Int. Conf. Robotics and Automation ICRA '09*, 2009, pp. 1402–1409.
14. M. A. Bicchi A., Pratichizzo D. and B. A, "On the observability of mobile vehicles localization," in *IEEE Mediterranean Conference on Control and Systems*, 1998.
15. G. Huang, A. Mourikis, and S. Roumeliotis, "Analysis and improvement of the consistency of extended kalman filter based SLAM," in *Proc. IEEE International Conference on Robotics and Automation ICRA 2008*, 2008, pp. 473–479.
16. A. Martinelli and R. Siegwart, "Observability analysis for mobile robot localization," in *Proc. IEEE/RSJ International Conference on Intelligent Robots and Systems (IROS 2005)*, 2–6 Aug. 2005, pp. 1471–1476.
17. M. Betke and L. Gurvits, "Mobile robot localization using landmarks," *IEEE Transaction for Robotics and Autonomus Systems*, vol. 13, no. 2, pp. 251–263, 1997.
18. L. D. L. Perera, A. Melkumyan, and E. Nettleton, "On the linear and nonlinear observability analysis of the SLAM problem," in *Proc. IEEE Int. Conf. Mechatronics ICM 2009*, 2009, pp. 1–6.
19. K. W. Lee, W. S. Wijesoma, and I. G. Javier, "On the observability and observability analysis of SLAM," in *Proc. IEEE/RSJ Int Intelligent Robots and Systems Conf*, 2006, pp. 3569–3574.
20. A. Mourikis and S. Roumeliotis, "Performance analysis of multirobot cooperative localization," *IEEE Transaction for Robotics and Autonomus Systems*, vol. 22, no. 4, pp. 666–681, 2006.
21. Y. Song and J. W. Grizzle, "The extended kalman filter as a local asymptotic observer for descrete -time nonlinear systems," *Journal of Mathemetical Systems, Estimation, and Control*, vol. 5, pp. 59–78, 1995.
22. R. Hermann and A. Krener, "Nonlinear controllability and observability," *IEEE Transactions on Automatic Control*, vol. 22, no. 5, pp. 728–740, Oct 1977.
23. V. K. Ethan Stump, Ali Jadbabaie, "Connectivity management in mobile robot teams," in *IEEE International Conference on Robotics and Automation*, 2008.
24. *https://sites.google.com/site/rajnikantwiki/research/cooperative-localization*.